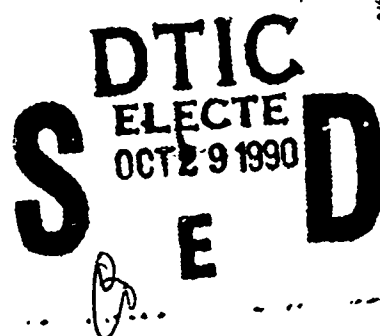RADC-TR-89-391
In-House Report
January 1990

AD-A227 965

STATISTICALLY THINNED ARRAYS WITH QUANTIZED ELEMENT WEIGHTS

Robert J. Mailloux and Edward Cohen

DTIC
ELECTE
OCT 29 1990
S E D

Rome Air Development Center
Air Force Systems Command
Griffiss Air Force Base, NY 13441-5700

This report has been reviewed by the RADC Public Affairs Division (PA) and is releasable to the National Technical Information Service (NTIS). At NTIS it will be releasable to the general public, including foreign nations.

RADC-TR-89-391 has been reviewed and is approved for publication.
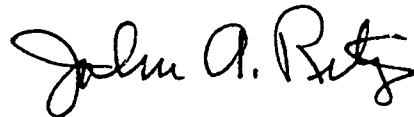
APPROVED:

ROBERT J. MAILLOUX
Chief, Antennas & Components Division
Directorate of Electromagnetics

APPROVED:

JOHN K. SCHINDLER
Director of Electromagnetics

FOR THE COMMANDER:

JOHN A. RITZ
Directorate of Plans & Programs

If your address has changed or if you wish to be removed from the RADC mailing list, or if the addressee is no longer employed by your organization, please notify RADC (EEA) Hanscom AFB MA 01731-5000. This will assist us in maintaining a current mailing list.

Do not return copies of this report unless contractual obligations or notices on a specific document require that it be returned.

REPORT DOCUMENTATION PAGE

1a. REPORT SECURITY CLASSIFICATION Unclassified		1b. RESTRICTIVE MARKINGS N/A			
2a. SECURITY CLASSIFICATION AUTHORITY N/A		3. DISTRIBUTION / AVAILABILITY OF REPORT Approved for public release; distribution unlimited.			
2b. DECLASSIFICATION / DOWNGRADING SCHEDULE N/A					
4. PERFORMING ORGANIZATION REPORT NUMBER(S) RADC-TR-89-391		5. MONITORING ORGANIZATION REPORT NUMBER(S)			
6a. NAME OF PERFORMING ORGANIZATION Rome Air Development Center	6b. OFFICE SYMBOL (If applicable) EEA	7a. NAME OF MONITORING ORGANIZATION			
6c. ADDRESS (City, State, and ZIP Code) Hanscom AFB Massachusetts 01731-5000		7b. ADDRESS (City, State, and ZIP Code)			
8a. NAME OF FUNDING / SPONSORING ORGANIZATION	8b. OFFICE SYMBOL (if applicable)	9. PROCUREMENT INSTRUMENT IDENTIFICATION NUMBER			
8c ADDRESS (City, State, and ZIP Code)		10. SOURCE OF FUNDING NUMBERS			

	PROGRAM ELEMENT NO. 62702F	PROJECT NO. 4600	TASK NO. 14	WORK UNIT ACCESSION NO. 01

11. TITLE (Include Security Classification)

Statistically Thinned Arrays with Quantized Element Weights

12 PERSONAL AUTHOR(S)
Mailloux, R.J. and Cohen, E.

13a. TYPE OF REPORT In-house	13b. TIME COVERED FROM 11/30/87 TO 11/30/89	14. DATE OF REPORT (Year, Month, Day) 1990 January	15. PAGE COUNT 44

16. SUPPLEMENTARY NOTATION

17. COSATI CODES			18. SUBJECT TERMS (Continue on reverse if necessary and identify by block number)
FIELD	GROUP	SUB-GROUP	Antenna arrays
09	01		Pattern synthesis Thinned array antennas

19. ABSTRACT (Continue on reverse if necessary and identify by block number)

This report investigates the use of statistical thinning and quantized element weights to produce low sidelobe patterns using large circular array apertures. The major result of the analysis is a comparison of several thinning algorithms and the evaluation of sidelobe levels, gain and effective radiated power data for large, but otherwise arbitrary size arrays.

20 DISTRIBUTION/AVAILABILITY OF ABSTRACT ☐ UNCLASSIFIED/UNLIMITED ☒ SAME AS RPT ☐ DTIC USERS	21. ABSTRACT SECURITY CLASSIFICATION Unclassified	
22a. NAME OF RESPONSIBLE INDIVIDUAL Dr. Robert J. Mailloux	22b. TELEPHONE (Include Area Code) 617-377-3710	22c. OFFICE SYMBOL RADC/EEA

DD FORM 1473, JUN 86 *Previous editions are obsolete.*

Preface

This report represents the combined results of the authors individual investigations. Robert Mailloux conceived the project and completed the analysis of Methods 1 and 2 as well as formulas for all the basic array parameters. Edward Cohen performed the analysis of Method 3, wrote and debugged all computer programs and derived the asymptotic dependence in the Appendix.

Accession For		
NTIS GRA&I		X
DTIC TAB		☐
Unannounced		☐
Justification		

By
Distribution/

Availability Codes	
Dist	Avail and/or Special
A-1	

Contents

Illustrations

Statistically Thinned Arrays with Quantized Amplitude Weights

1. INTRODUCTION

Skolnik, et al[1], and others[2,3] have investigated the use of statistically designed density tapers to control antenna pattern sidelobes. In the procedure described by Skolnik, all of the elements of the array were excited with the same weights and the density of elements was made proportional to the amplitude of the aperture illumination of a conventional "filled" array. The resulting ensemble-averaged power pattern was shown to be equal to the sum of the filled array pattern and a distribution that was not angle-dependent, and which represented an average sidelobe level. A recent paper by Numazaki, et al[4] combines statistical thinning with a deterministic procedure to achieve improved patterns in pre-selected angular planes (the principal orthogonal planes and the diagonal planes). The authors also extended their procedure to address multiple quantized weights. The present work also addresses thinned arrays with multiple quantized weights, but is primarily concerned with

1. Skolnik, M., Sherman III, J.W., and Ogg, Jr., F.C. (1964) Statistically Designed Density - Tapered Arrays, *IEEE Trans. Antennas Propagat.* **AP-12**:408-411.

2. Lo, Y.T., (1964) A Mathematical Theory of Antenna Arrays with Randomly Spaced Elements, *IEEE Trans. Antennas Propagat.* **AP-12**:257-268.

3. Steinberg, B.D. (1972) The Peak Sidelobe of the Phased Array Having Randomly Located Elements, *IEEE Trans. Antennas Propagat.* **AP-20**(No. 2).

4. Numazaki, T., Mano, S., Kategi, T., and Mizusawa, M. (1987) An Improved Thinning Method for Density Tapering of Planar Array Antennas, *IEEE Trans. Antennas Propagat.* **AP-35** No. 9):1066-1069.

evaluating the ensemble-average array parameters for several quantizing algorithms. This study was motivated by the fact that if array amplitude weights are applied by solid state modules, then it is often practical and more economical to select modules with a small number of discrete, or quantized, amplitude levels, and to organize the array into annular rings with the quantized levels. Since an array with quantized amplitudes may produce high sidelobes, the goal of this study was to use statistical thinning to smooth the average amplitude illumination and reduce peak sidelobe levels. The changes in average sidelobe level gain and effective isotropic radiated power due to this design procedure were then evaluated.

## 2. METHODS OF STATISTICAL THINNING AND QUANTIZING

Several design procedures will be discussed that require an "ideal" continuous distribution as a starting point to synthesize the desired arrays. Figure 1a shows a representation of a continuous amplitude distribution that will be considered an ideal illumination designed to produce a low sidelobe pattern circular aperture. Throughout this report the aperture distribution will be represented by the circular Taylor patterns.[5] The circular aperture illumination will be sampled by a rectangular grid array (Figure 1c) with elements located 0.5λ apart, as done in the earlier Skolnik study. Figure 1b shows a step-wise continuous aperture distribution composed of three levels that define the set of available weights. By proper selection of the levels, which we refer to as amplitude or weight quantizations, and applying one of the three thinning procedures described below, one can approximate the ideal aperture illumination (A_n) and achieve low sidelobe average radiation patterns. Throughout much of this analysis we shall use Skolnik's notation, and denote aperture sums as one-dimensional sums over the index n while understanding this as a shorthand for the conventional two dimensional array summations.

The three thinning methods used in this study are depicted in Figure 2. The ideal aperture taper, indicated dashed, is approximated either by omitting elements entirely (thinning) or by selecting weight values from several discrete amplitude levels in accordance with statistical rules to be described. Following Skolnik, the mathematical treatment will include not only the important case called "Natural Thinning", in which the aperture element density varies from unity (filled) to low (sparsely filled) in an attempt to approximate the desired weighting, but will also consider thinning beyond this "natural" range. The density of elements is thus scaled by a constant $k \leq 1$ such that the probability of any element being excited can be $\leq k$ (instead of unity) while the ideal aperture distribution remains proportional to the naturally thinned case ($k = 1$). Throughout this report, the analysis will account for $k < 1$, but the examples will be restricted to natural thinning.

5. Taylor, T.T. (1960) Design of Circular Apertures for Narrow Beamwidth and Low Sidelobes, *IRE Trans.* **AP-8**:23-26.
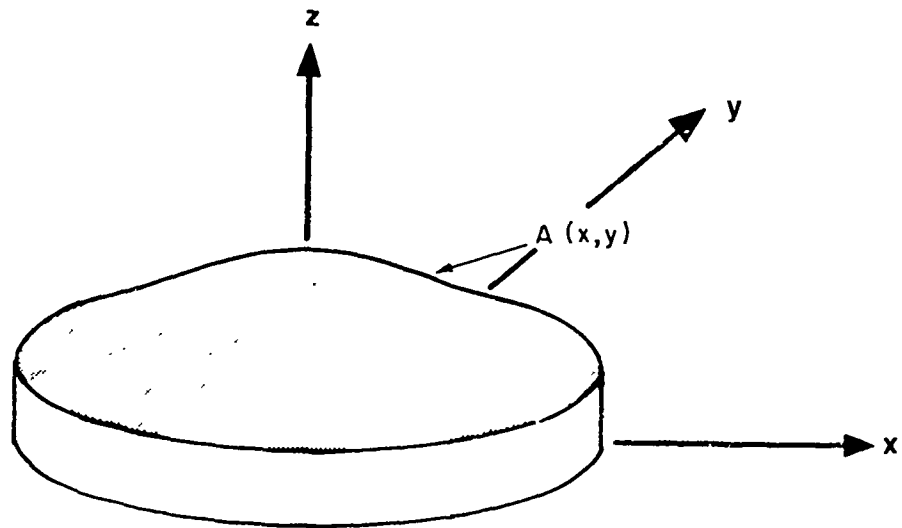
A. ARRAY AMPLITUDE TAPER A(x,y)
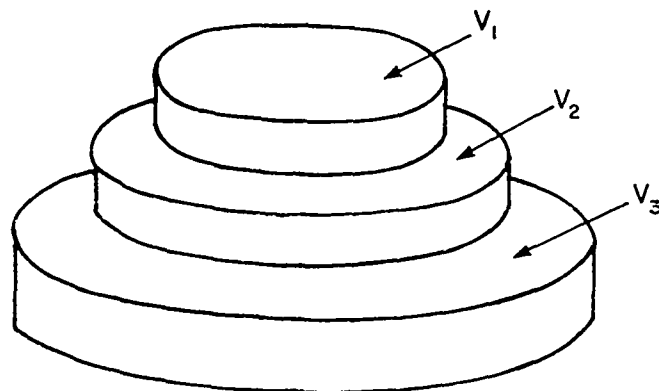
B. QUANTIZED AMPLITUDE TAPER
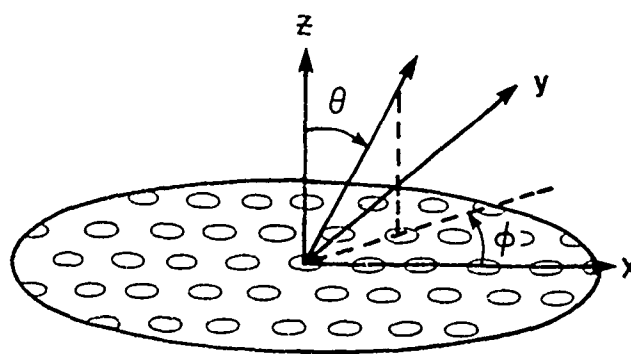
C. ARRAY APERTURE AND COORDINATES

Figure 1. Array Amplitude Taper

ARRAY
AMPLITUDE
TAPER
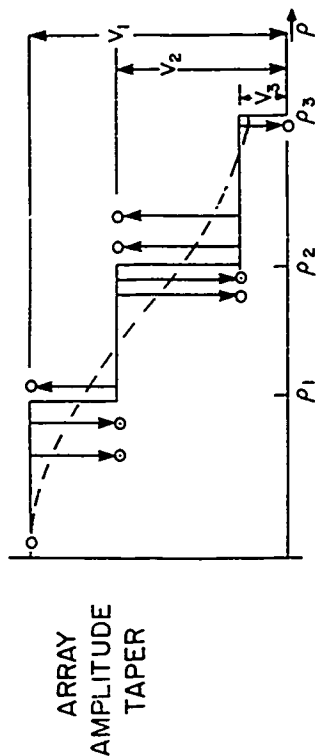
METHOD 3: IN ANNULUS $\rho_{p-1} < \rho < \rho_p$

WEIGHTS F_n ARE A COMBINATION

OF V_{p-1} AND V_p OR V_{p+1}, AND V_p

o = WEIGHT VALUE AFTER THINNING
    e.g. V_1, V_2, V_3, OR 0

⌐ = TAYLOR TAPER

⌐_ = STAIRCASE ILLUMINATION OR APODIZATION

$\rho = r/a$

ARRAY
AMPLITUDE
TAPER
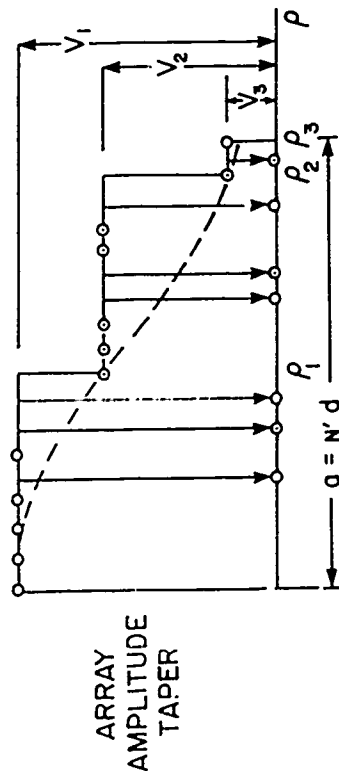
METHOD 1

IN ANNULUS $\rho_{p-1} < \rho < \rho_p$, WEIGHTS F_n ARE V_p OR ZERO

ARRAY
AMPLITUDE
TAPER
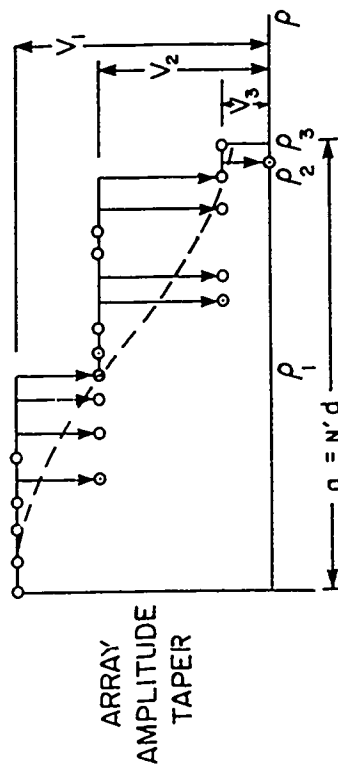
METHOD 2

IN ANNULUS $\rho_{p-1} < \rho < \rho_p$, WEIGHTS F_n ARE V_p OR V_{p+1}

Figure 2. (a) Ideal Taper (Dashed) and Method 1 Source Weight Options (b) Ideal Taper (Dashed) and Method 2 Source Weight Options (c) Ideal Taper (Dashed) and Method 3 Source Weight Options

4

2.1 Description of Methods

2.1 1 METHOD 1

Method 1 of Figure 2a shows the simplest combination of thinning with amplitude quantization: Discrete weights V_p are chosen, always above the ideal illumination envelope, (except at the origin) and sources are either left "on" or turned completely "off" in accordance with an algorithm that makes the azimuthally averaged amplitude at any radial position nearly that of the taper. The probability of assigning the weight $F_n = V_p$ to an element at location ρ_n in the radial annulus $\rho_{p-1} \leq \rho \leq \rho_p$ is given by:

$$P\{F_n = V_p\} = kA_n/V_p \tag{1}$$

where A_n is the amplitude of the ideal illumination at the nth element. The probability of turning the element off is $[k-P(V_p)]$. The figure indicates that some elements are left on at the value V_p while others are set to zero. In terms of a distribution around some annular ring of elements, the above result also indicates that the average of the weights around a large ring of elements will also be given by kA_n/V_p. In principle, there can be many discrete levels, although in practice some small number will be chosen.

2.1.2 METHOD 2

In Method 2, the staircase of discrete levels is again kept above, or just touching the ideal envelope A_n, but in this case the average level for a ring of sources is attained by also exciting some fraction of elements with the next lower level of amplitude. Since the next discrete level is also available to a solid state module, it would seem reasonable to take advantage of this added degree of freedom instead of restricting oneself to the on-off devices in Method 1. For Method 2, whether considered from an average over an ensemble of arrays, or counted from the annulus of a large array, if there are M_2 elements at the level V_p, M_1 elements at the next lower level V_{p+1} and still others missing or turned off, then for the average level to be A_n, one requires:

$$\frac{M_2}{M_1 + M_2} V_p + \frac{M_1}{M_1 + M_2} V_{p+1} = A_n . \tag{2}$$

Since the total excitation probability is k, to account for generalized thinning,

$$P(F_n = V_p) + P\{F_n = V_{p+1}\} = k . \tag{3}$$

We associate the probability of exciting elements at levels V_p and V_{p+1}, respectively, with

$$P(F_n = V_p) = k \frac{M_2}{M_1 + M_2} , \quad P(F_n = V_{p+1}) = k \frac{M_1}{M_1 + M_2} . \tag{4}$$

Solving for the probabilities yields

$$P\{F_n = V_p\} = k \frac{[A_n - V_{p+1}]}{V_p - V_{p+1}} , \quad P(F_n = V_{p+1}) = k \frac{[V_p - A_n]}{V_p - V_{p+1}} . \tag{5}$$

The sketch illustrating Method 3 looks quite different from that of Method 2, but in fact the only geometrical difference is in the selection of radii ρ_p. In Method 3, the staircase of discrete levels is not kept above the envelope, but is roughly half below and half above the taper at $A(\rho_p)$. If a particular ρ_p is

selected, the step height is chosen so that it is bisected by the A (ρ_p), that is, A $(\rho_p) = 1/2 (V_p + V_{p+1})$. This choice is arbitrary and can lead to inferior results for cases with very few steps, as will be discussed in Section 4.4. Method 3 must contend with current sources in circles or annuli for which A_n lies either above the bisected staircase or below it. The consequence is that two sets of probability densities are needed to implement the method, as will now be discussed.

2.1.3 METHOD 3

In Figure 3, a section of the Method 3 configuration has been expanded. Sources at grid locations denoted by n_1 and n_2 are displayed. The value of the weight at n_1, n_2, namely, $F_{n_{1,2}}$ are allowed to take either of two values:

$$F_{n1} = V_p \text{ or } V_{p+1} ; \quad F_{n2} = V_{p-1} \text{ or } V_p \tag{6}$$

The probabilities for F_n assuming one of the two values are defined below by the "relative" closeness of A_n to a level. (See Figure 3)

Region (I)   Step <u>above</u> taper

$$P(F_{n1} = V_p) = k \frac{[A_{n1} - V_{p+1}]}{[V_p - V_{p+1}]} ; \quad P(F_{n1} = V_{p+1}) = k - P(F_{n1} = V_p) \tag{7}$$

Region (II)   Step <u>below</u> taper

$$P(F_{n2} = V_p) = k \frac{[V_{p-1} - A_{n2}]}{[V_{p-1} - V_p]} ; \quad P(F_{n2} = V_{p-1}) = k - P(F_{n2} = V_p) \tag{8}$$
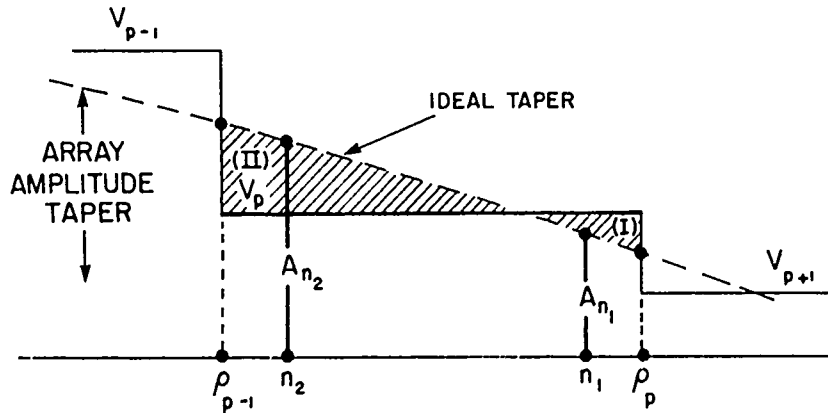

Figure 3. Expanded View of Method 3 Geometry

Intuitively, as A_n approaches V_p, the probability should increase that the weight F_n at the source location ρ_n assumes the value V_p. Thus, drawing a uniformly distributed random variate (rv) from a pseudo-random-number generator producing samples over $0 \leq rv \leq k$ lets one decide on the value given to F_n. For example, suppose a source element is located at ρ_{n_2}, a position where the taper amplitude *exceeds* the level value (in this case V_p). If, say $P(F_{n2} = V_p) = 0.85$ one would set $F_{n2} = V_{p-1}$ for $rv \leq 0.85$. Using the probability formulas for Methods 1 and 2, respectively, one can decide in a similar fashion whether to set $F_n = V_p$ or 0 and $F_n = V_p$ or $V_p + 1$. The thinning algorithms for all three methods were constructed using this design philosophy.

2.2 Average Power Patterns of Thinned, Quantized Arrays

If the ideal aperture taper of Figure 1 were sampled periodically, and radiated from a filled, periodic array, the sampled values A_n would radiate to produce the far field pattern

$$E_0(\theta,\phi) = \sum_{n=1}^{N} A_n \exp(j \Phi_n) \tag{9}$$

where the $\Phi_n(\theta,\phi)$ is the phase factor as detailed in Section 4. In the case of the new array with a finite set of amplitudes and the source configuration subjected to statistical thinning, the field intensity pattern is written:

$$E(\theta,\phi) = \sum_{n=1}^{N} F_n \exp(j \Phi_n) \tag{10}$$

where the F_n are selected randomly in accord with the previously described rules.

Ensemble averaging the field intensity, $E(\theta,\phi)$, from many thinned arrays leads one to set

$$\overline{F}_n = kA_n \tag{11}$$

in order to have

$$\overline{E(\theta,\phi)} = kE_0(\theta,\phi) \tag{12}$$

For large arrays, we assume that the azimuthal sample average of the F_n is nearly the same as the ensemble average; namely that

$$< Fn > = \overline{F}_n = kA_n . \tag{13}$$

For the purpose of deriving averaged expressions, the ensemble average is more convenient to invoke. The mean value of the field strength is thus given by

$$\overline{E(\theta,\phi)} = \overline{\sum_{n=1}^{N} F_n \exp(j \Phi_n)} = \sum_{n=1}^{N} \overline{F}_n \exp(j \Phi_n) \tag{14}$$

$$= kE_0(\theta,\phi)$$

which is the pattern of the ideal, filled array.

7

The power pattern is the absolute square of the field intensity pattern. Following Skolnik, the power pattern is:

$$\overline{|E(\theta,\phi)|^2} = E(\theta,\phi)\, E^*(\theta,\phi) \tag{15}$$

$$= \Sigma\Sigma\, F_m F_n \exp[j(\Phi_m - \Phi_n)]$$

and

$$\overline{|E(\theta,\phi)|^2} = \overline{\Sigma F_n^2} + \overline{\sum_{\substack{m \\ m \neq n}} \sum_{n} F_m F_n \exp[j(\Phi_m - \Phi_n)]}$$

is its expected value for real F_n. The $m = n$ index is separated out to invoke the theorem from statistics which states that for statistically independent random variables, the mean of a product is the product of the means.

2.2.1 METHOD 1

At this point the analysis departs from that of Skolnik to address the specific algorithms under study. First, it is convenient to break up the sums over n into groups that correspond to the discrete levels. Thus, a sum over n for the entire array is written as a double sum over the elements at all P levels, with the index n varying between N_{p-1} and N_p in the pth level (that level between P_{p-1} and P_p):

$$\sum_{n=1}^{N_T} = \sum_{p=1}^{P} \sum_{n(p)} \tag{16}$$

The Quantities F_n can assume either of two values, V_p or O, for n in the region $N_{p-1} < n < N_p$. Using the definition for the mth moment of a discrete probability density function (PDF),

$$\overline{X^m} = \sum_i x^m\, P[x_i = x], \tag{17}$$

one gets from Eq. (1)

$$\overline{F_n^2} = V_p^2\,(kA_n/V_p) + O \tag{18}$$

for i = 1 and 2, leading to

$$\overline{\sum_n F_n^2} = k\, \sum_p V_p \sum_{n(p)} A n\,. \tag{19}$$

The second term of Eq. (15) is evaluated below using the theorem concerning the mean of the product of statistically independent variables.

$$\overline{\sum_{\substack{m \\ m \neq n}} \sum_n F_m F_n \exp[j(\Phi_m - \Phi_n)]} \tag{20}$$

$$= \sum_{\substack{m \\ m \neq n}} \sum_n (\overline{F_m}\ \overline{F_n}\ \exp[j(\Phi_m - \Phi_n)]$$

Using Eq. (13), this becomes

8

$$\sum_{\substack{m \\ m \neq n}} \sum_n k^2 A_m A_n \exp \left[j \left(\Phi_m - \Phi_n\right)\right] \tag{21}$$

$$= k^2 |E_0(\theta,\phi)|^2 - k^2 \sum_n (A_n)^2$$

Combining both sums to produce the average power result leads to:

$$|\overline{E(\theta,\phi)}|^2 = k^2 |E_0(\theta,\phi)|^2 + \sum_p V_p \sum_{n\ (p)} k A_n \left(1 - k A_n / V_p\right)$$

$$= k^2 |E_0(\theta,\phi)|^2 + P_{SL} \tag{22}$$

where

$$P_{SL} = \sum_p V_p \sum_{n\ (p)} k A_n \left(1 - k A_n / V_p\right) .$$

The expression is similar to Skolnik's result in that it has two terms: the first is the power pattern of the ideal filled array, and the second is a constant or uniform level independent of the angle variables θ and ϕ. It is a generalization of Skolnik's result, and reduces exactly to it if there is only a single level V_0 and not a set of discrete levels. Quantitative results from the method will be discussed in a later section.

2.2.2 METHOD 2

Using the probabilities given in Eq. (5), we have from the moment formula for F_n^2:

$$\overline{(F_n)^2} = (V_p)^2 \frac{k[A_n - V_{p+1}]}{V_p - V_{p+1}} + (V_{p+1})^2 \frac{k[V_p - A_n]}{V_p - V_{p+1}} \tag{23}$$

Summing over all n, and using the double sum notation described for method 1, we arrive at

$$\overline{\sum_n (F_n)^2} = k \sum_p \sum_{N_{p-1}}^{N_p} [A_n (V_p + V_{p+1}) - V_p V_{p+1}]. \tag{24}$$

The second term of the average power pattern is again given by Eq. (21), as can also be verified by inserting the expression for F_n into this term and using the probability formulas (Eq. 5) for Method 2. Collecting terms, we get the final result:

$$|\overline{E(\theta,\phi)}|^2 = k^2 |E_0(\theta,\phi)|^2 - \sum_n k^2 (A_n)^2$$
$$+ k \sum_p \sum_{N_{p-1}}^{N_p} [A_n (V_p + V_{p+1}) - V_p V_{p+1}] . \tag{25}$$

Clearly this is in the form of Eq. 22, with the average sidelobe level

$$P_{SL} = \sum_p \sum_{n(p)} [k A_n (V_p + V_{p+1}) - V_p V_{p+1}] - \sum_n k^2 (A_n)^2 \tag{26}$$

2.2.3 METHOD 3

The probabilities for Method 3 have been defined in Eq. (7) and (8). Again, the ensemble averaged power pattern is given by $E(\theta, 0)^2$ shown in Eq. (15). The major difference between Method 3 averaging and the others is that now one has to split the sum over n into two parts, namely,

$$\overline{\sum_n (F_n)^2} = \overline{\sum_{(1)} (F_{n1})^2} + \overline{\sum_{(2)} (F_{n2})^2} \tag{27}$$

where the (1) and (2) denote the two regions and options encountered in a typical interval (ρ_{p-1}, ρ_p). Using Eqs. (6) and (7) for the probability densities, and Eq. (17) for the first moment, we obtain for Region 1

$$\overline{F_{n1}} = V_p \frac{k(A_{n1} - V_{p+1})}{V_p - V_{p+1}} + V_{p+1} \frac{k(V_p - A_{n1})}{V_p - V_{p+1}} \ . \tag{28}$$

For Region 2,

$$\overline{F_{n2}} = V_p \frac{k(V_{p-1} - A_{n2})}{V_{p-1} - V_p} + V_{p-1} \frac{k(A_{n2} - V_p)}{V_{p-1} - V_p} \tag{29}$$

Next, we will need to consider the second moments. For Region (1),

$$\overline{(F_{n1})^2} = (V_p)^2 P(F_{n1} = V_p) + (V_{p+1})^2 P(F_{n1} = V_{p+1}) \ ; \tag{30}$$

similarly, for Region (2):

$$\overline{(F_{n2})^2} = (V_p)^2 P(F_{n2} = V_p) + (V_{p-1})^2 P(F_{n2} = V_{p-1}) \ . \tag{31}$$

Collecting contributions from all P intervals, namely, for the entire array, gives

$$\overline{|E(\theta,\phi)|^2} = \sum_n \overline{(F_n)^2} + \sum_{\substack{n \\ m \neq n}} \sum_m \overline{F}_m \overline{F}_n \exp j(\Phi_n - \Phi_m) \tag{32}$$

which again may be written as

$$= \sum_n \overline{(F_n)^2} + k^2 \left| E_0(\theta,\phi) \right|^2 - k^2 \sum_n (A_n)^2 \tag{33}$$

Substituting the probability formulas into the equations simplifies the results to

$$\overline{|E(\theta,\phi)|^2} = k^2 |E_0(\theta,\phi)|^2 - k^2 \sum_n (A_n)^2$$

$$+ k \sum_p \left\{ \sum_{(1)} [A_{n1} (V_p + V_{p+1}) - V_p V_{p+1}] \right.$$

$$\left. + \sum_{(2)} [A_{n2} (V_p + V_{p-1}) - V_p V_{p-1}] \right\} \tag{34}$$

The average sidelobe level for Method 3 is thus given by

$$P_{SL} = -k^2 \sum_n A_n^2 + k \sum_{(1)} \left\{ \Sigma [A_{n1} (V_p + V_{p+1}) - V_p V_{p+1}] \right.$$

$$\left. + \sum_{(2)} [A_{n2} (V_p + V_{p-1}) - V_p V_{p-1}] \right\} . \tag{35}$$

3. ARRAY PARAMETERS

The several expressions obtained above give average patterns that have two terms; the ideal filled array pattern, and an average pattern independent of angular variation. At first glance it appears from these expressions that one need only evaluate the average (far sidelobe) patterns to compare the results of the three thinning methods; however, there are other array parameters that depend upon the quantization and thinning. They are evaluated in this section and described in a number of figures that follow. The chosen array is laid out on a rectangular grid, with inter-element spacings of 0.5 λ in each direction, the array radius for the pth annular ring being ρ_p. Within each ring there are a fixed number of elements, and the several methods differ in the way they perform the statistical thinning and quantizing for each ring.

3.1 Normalized Input Power

If there are a total of N elements in the array with amplitudes F_n, then the total power into the array, normalized to the input power into a uniformly illuminated filled array ($F_n = 1$) is:

$$P_{in} = \frac{\Sigma (F_n)^2}{N} . \tag{36}$$

P_{in} is shown in Figures 9a, 10a, 11a for the three methods.

3.2 Average Sidelobe Levels

The (ensemble) average sidelobe power levels P_{SL} given in Eqs. (22), (28) and (37) should be normalized to the ensemble average peak of the radiated signal. For convenience however, it has been normalized to the peak of the specific designed array or $(\Sigma F_n)^2$. The average sidelobe level normalized to the beam peak is given below:

$$SL = \frac{P_{SL}}{(\Sigma F_n)^2} \tag{37}$$

3.3 Array Directivity

The directivity of an array depends upon the element pattern, and does not admit to a closed form expression in that it needs to include mutual coupling terms explicitly; otherwise one must resort to an integration of the entire pattern. Skolnik uses a formula that neglects mutual coupling (and assumes a unity gain element pattern) to obtain:

11

$$D = \frac{\left|\Sigma F_n\right|^2}{\Sigma \left|F_n\right|^2} \tag{38}$$

One interesting point about Eq. (38) is that it is not sensitive to the (ensemble) average sidelobe level or the relative degree of thinning. For a single discrete level with each F_n either one or zero, the directivity is just the number of non-zero biased elements, independent of the array size or degree of thinning, even though the average sidelobe level may have increased to a degree where it should dominate the directivity. Put another way, this formula says that an array of N elements, excited with equal amplitudes, has the same gain for any array spacing, as long as the mutual coupling can be neglected. As written, the formula implies a unity gain (omnidirectional) element pattern, and so one can argue that for a very sparse array the gain should be multiplied by 2 to account for hemispherical radiation (while still neglecting coupling). When the array elements are closely spaced (say about 0.5 λ) then clearly the array directivity for the uniformly excited filled array has to approach the area directivity $(4\pi A/\lambda^2)$, and one can show this as being consistent with Eq. (38) only if an element directivity of π is assumed to multiply Eq. (38).

One can, in fact, show that if the element patterns of an array are identical (no end effects) then the array directivity can be written

$$D = D_e \frac{\left|\Sigma F_n\right|^2}{\Sigma \left|F_n\right|^2} \tag{39}$$

and the only problem with the above formula is that the element pattern D_e varies between π for a filled array lattice (with unexcited elements terminated) and 2 for an array with hemispherical element patterns.

In the present study, we wish to address several cases in which the array is nearly filled, and have introduced an expression for the average directivity of a statistically thinned array radiating into a half-space. For all three methods the ensemble average pattern of the array takes the form:

$$\overline{E(\theta,\phi)^2} = k^2 \left|E_0(\theta,\phi)\right|^2 + P_{SL} \tag{40}$$

where the $|E_0(\theta, \phi)|^2$ is the ideal pattern of the tapered, filled array. The directivity of an antenna radiating into a half-space is given by

$$D = \frac{4\pi \, P_{max}}{\displaystyle\int_\Omega P(\theta,\phi) \, d\Omega} \tag{41}$$

where P_{max} is the power density $k^2 |E_0|_{max}$ at the beam peak, Ω is the solid angle subtended in the upper half-space, and $d\Omega = \sin\theta \, d\theta d\phi$.

The average directivity in this case is:

$$D = \frac{4\pi}{\displaystyle\int k^2 \left|E_0(\theta,\phi)\right|^2 d\Omega + \frac{P_{SL}}{P_{max}} \int d\Omega} = \frac{D_0}{1 + 1/2 \, k^{-2} \, D_0 \, SL} \tag{42}$$

for the sidelobe level $SL = P_{SL}/P_{max}$ and D_0 is the directivity of the ideal pattern.

Eq. (42) shows that the average directivity depends on the ideal pattern directivity and the average sidelobe level. When the average sidelobe level approaches zero, as for the filled ideal aperture taper, the directivity tends to the correct limit [of $4\pi(A/\lambda^2 \varepsilon_{ap})$] where ε_{ap} is the aperture efficiency of the chosen distribution (in this case the circular aperture Taylor distribution). When the average sidelobes are at the isotropic level, the directivity is reduced by about 1.8 dB (SL = $1/D_0$). For very high average sidelobes, the directivity approaches 2/SL above the sidelobe level, which is the case when virtually all the power is in the average sidelobes and the radiation is contained in a half-space. Notice that the thinning constant k does not enter explicitly in this formula, but is included in a sidelobe level.

The expression (42) is not exact, for it implies an omnidirectional (half-space) element pattern applied to the integration of the average sidelobe power in the dominator of Eq. (41), and so neglects element pattern changes due to coupling. If it is assumed that the array elements are closely spaced, a $\cos \theta$ element pattern might be assumed to modify the average sidelobe power integral. That would lead to a factor of 1/4 multiplying the term SL for this case of very little thinning. However, in that limit the average sidelobes are very low and the directivity very nearly the ideal (so it doesn't matter what element pattern is used). Alternatively, when the array is highly thinned, the element pattern is more nearly omnidirectional (in the hemisphere), and expression (42) should then be a good approximation. The validity of it was tested by integrating the directivity formula (41) assuming ϕ symmetry, for several cases as noted on the figures.

3.4 Normalized EIRP (Effective Isotropic Radiated Power)

The product of normalized input power and array (average) gain is an Effective Isotropic Radiated Power (or EIRP). The EIRP is one of the primary measures of the antenna system, as it produces the power density at the target (or receiver). For a lossless antenna system the directivity and gain are equal and,

$$EIRP = D \, P_{in} \tag{43}$$

4. ARRAY CALCULATIONS AND RESULTS

4.1 Array Pattern Calculations

The array factor for a circular aperture array with elements located on a rectangular grid is:
$$E(\theta,\phi) = K \Sigma \Sigma \, F_{mn} \exp \{ j(2\pi/\lambda) \, [md_x (u - u_0) + nd_y (v - v_0)] \}$$
for

$$u = \sin \theta \cos \phi; \; u_0 = \sin \theta_0 \cos \phi_0$$

$$v = \sin \theta \sin \phi; \; v_0 = \sin \theta_0 \sin \phi_0 \tag{44}$$

for m and n within the circular planar region as shown in Figure 1, and elements centered at the locations $(x_m, y_n) = (md_x, nd_y)$.

The constants F_{mn} are real and are determined from the statistical algorithms given in previous sections. The constant K is chosen to produce max $F(\theta, \phi) = 1$; namely

13

$$K = 1/(\Sigma \ \Sigma \ | \ F_{mn} |) \tag{45}$$

Since the array investigated in this paper contained several thousand elements, the circular Taylor amplitude distribution [Ref 5] (characterized by the parameter $\bar{n}$) had to be sampled thousands of times at the nodes of a rectangular grid locating the current elements. To speed the process of evaluating the Taylor function, we sampled it at 19 positions across its radius and used a cubic spline code for rapid interpolation at the grid radii, r (x_m, y_n), leading to significant reductions in program execution time.

The Taylor illumination being emulated was always chosen with $\bar{n}$ as a large as possible while maintaining monotonically decreasing current distributions from the origin. This selection leads to the highest aperture efficiency and narrowest beamwidth subject to given sidelobe criteria while maintaining realistic taper illuminations. The selected values of $\bar{n}$ accompanied by their computed aperture efficiencies are given below:

Sidelobe Level (dB)	$\bar{n}$	Efficiency
-30	5	0.8623
-35	6	0.7880
-40	7	0.7186
-45	9	0.6620
-50	11	0.6106
-55	13	0.5651
-60	15	0.5251
-65	18	0.4909
-70	21	0.4603
-75	23	0.4325

These efficiencies were calculated from Hansen[6] using

$$\varepsilon = \left\{ 1 + \sum_{n=1}^{\bar{n}-1} \frac{F_n^2}{J_0^2 (\pi \mu_n)} \right\}^{-1} \tag{46}$$

where the μ_n are the zeros of $J_1(\pi\mu)$.

These efficiencies were used in the computation of directivity for the ideal pattern using:

$$D_0 = \frac{4\pi A}{\lambda^2} \varepsilon \tag{47}$$

The pattern calculations for a filled, sampled aperture of this size are very nearly identical to those of the continuous aperture with the Taylor taper and so exhibit sidelobes at the design level.

4.2 The Design Process

Since the objective is to apply statistical thinning methods to a sampled, step-wise continuous aperture illumination, the following question arises: What amplitude levels (V_p) and radii (ρ_p) are to be assigned to the steps? Ideally, according to some criteria, the best (V_p, ρ_p) is determined and the

6. Hansen, R.C. (1983) *The Handbook of Antenna Design*, Vol 2, Chapter 10, pp. 157, Rudge et. al. (Editors), Peter Peregrinius Ltd.

array is thinned, *simultaneously*. The inherent difficulties of global optimization in this context leads us to the (suboptimal) design scheme described below. In it, the best (ρ_p) is determined first, and then the array is thinned.

We assume that by approximating the ideal taper with the staircase function shown in Figure 1c, Taylor power pattern features will emerge as the number of steps (P) increases indefinitely. To choose the "best" power pattern for a small number (P) of steps we proceed as follows:

1. N sets of randomly generated ρ_p are created;

    ' Corresponding sets of V_p are obtained by evaluating the Taylor taper at the ρ_p;

3. The power patterns for all N staircase apodizations are calculated;

4. The interval containing the first few Taylor sidelobes (in each power pattern) is sampled and the number of ordinates (Q) *exceeding* the design sidelobe level (SLL) is counted; and finally,

5. The staircase parameters (ρ_p, V_p) yielding the smallest Q is deemed the best for the subsequent thinning operations.

Typically, N = 200 configurations were considered.

The power patterns required in Step 3 are easily calculated using the two-dimensional Fourier transform over the circular aperture with constant illumination in each ring. By virtue of the rotational symmetry, one is led to the evaluation of a finite Hankel transform for each ring. For P steps in the staircase, the far-field amplitude distribution becomes

$$F_s(\sin\theta) = C\ \Sigma[V_p - V_{p+1}]\ (\rho_p)^2\ \frac{\{J_1(2\pi\rho_p\ \sin\theta)\}}{2\pi\rho_p\ \sin\theta} \tag{48}$$

with C a normalization and $\rho_p = r_p/\lambda$, $V_{p+1} = 0$, F_s^2 gives the required power pattern.

Some of the best patterns, obtained for various specifications of desired sidelobe level, were those for which the radii varied as

$$\rho_p \simeq p\Delta\rho \qquad\qquad p = 1,2,3...$$

for Methods 1 and 2. For Method 3, no simple relationship governing the radii could be inferred.

Having obtained the implied ρ_p, the three algorithms were run to evaluate the patterns as well as to determine how the basic parameters - gain, average sidelobe level and normalized EIRP - varied with method. The results are summarized in Figures 9 through 14.

4.3 Array Dimensions and Generalizations

In nearly all cases the data was taken for the following array dimensions:

> Array Diameter: 51 λ
> Element Spacing: 0.5 λ (square grid)
> No. of Elements in Filled Array: 7845
> Design Sidelobe Level (dB): -30 to -75

Although most data was collected for only one array, it is possible to infer the average parameters of other large arrays. It is shown in the Appendix that for a large array with a given taper, the normalized sidelobe level varies as 1/N, where N is the total number of array elements. The array directivity varies directly with N. This means that the product N SL and the quotient D/N are

constants, independent of array size, once the arrays are sufficiently large. For this reason the curves in Figures 9 through 14 are generalized with ordinates on the left that include the array element count N, while the ordinates at the right of each figure are the actual computed data. The ordinates of the sidelobe curves are given a normalized sidelobe level that is the product of N times the sidelobe ratio.

$$10 \log_{10} SL_{norm} = 10 \log_{10} SL + 10 \log_{10} N$$

The ordinate of the normalized EIRP curve is:

$$10 \log_{10} D_{norm} = 10 \log_{10} D - 10 \log_{10} N$$

The ordinate of the normalized EIRP curve is:

$$10 \log_{10} (EIRP_{norm}) = 10 \log_{10} EIRP_{watts} - 20 \log_{10} N$$

Since N was 7845 elements, the parameter 10 log N is + 39 dB.


4.4 Discussion of Results

Figure 4a shows the power pattern resulting from a discrete array of elements located at the nodes of a rectangular sampling grid $(x_m, y_m: \Delta_x = \Delta_y = 0.52)$ within the circular aperture. The grid samples a -50dB Taylor taper, with amplitude A (r_{mn}) for

$$(r_{mn} = \sqrt{x_m^2 + y_n^2});$$

the pattern is clearly a good approximation to that arising from the unsampled A(r).

Figure 4b shows the pattern of a filled array with three discrete amplitude levels used to approximate a -50dB Taylor illumination (see Figure 1c). The amplitude levels (w) and quantization step radii (ρ) are shown in this Figure, as well as in those that follow. Since the array is not thinned there are some relatively high sidelobes, but the annular distribution of the discrete amplitude levels tends to minimize grating lobes. The goal of this study is to improve this and similar patterns by utilizing various statistical thinning procedures in addition to the discrete level approximation to the taper.

Figure 5a shows the result of thinning the array using the same excitation amplitude at all elements and statistically thinning the array (as done by Skolnik) to match the -50 dB Taylor taper illumination. Clearly the pattern has the correct beam width, but has many sidelobes above the -35dB level and average sidelobes at -37.5 dB. The pattern directivity is 36.2 dB. The degree of thinning is indicated in Figure 5b, which shows a continuous grading of elements removed to approximate the desired density taper. In this figure the dashed lines indicate elements that are not excited. Notice that the attempt to match an exceedingly low sidelobe taper has led to very inefficient use of the aperture and to high average sidelobes. This is a rather extreme example, because if the array had been larger (by a factor of 10 for example) then the average sidelobes in Figure 5a would be reduced another 10 dB. As shown by Skolnik, the average sidelobe level is approximately 1/N for highly thinned arrays. Figures 6, 7, and 8 show the same example with three steps of amplitude illumination. For comparison, recall that Figure 4b shows the optimized three-step-pattern without thinning and indicates peak sidelobes in the neighborhood of -27 dB. In 7b and 8b dashed lines indicate that the
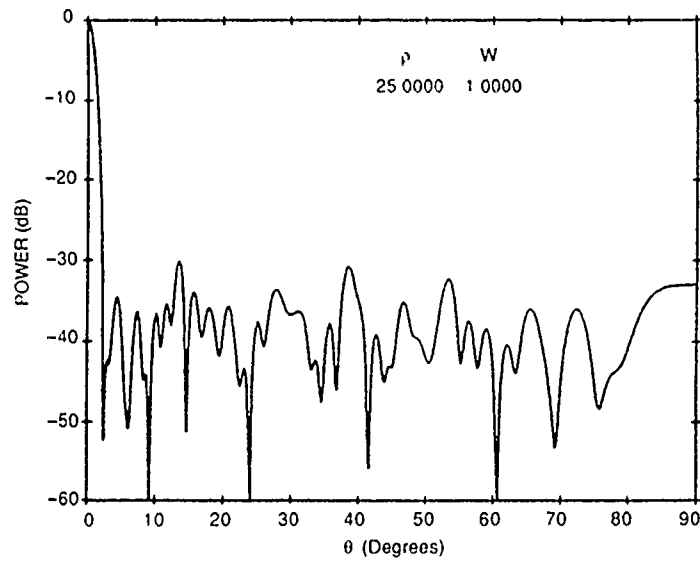
16
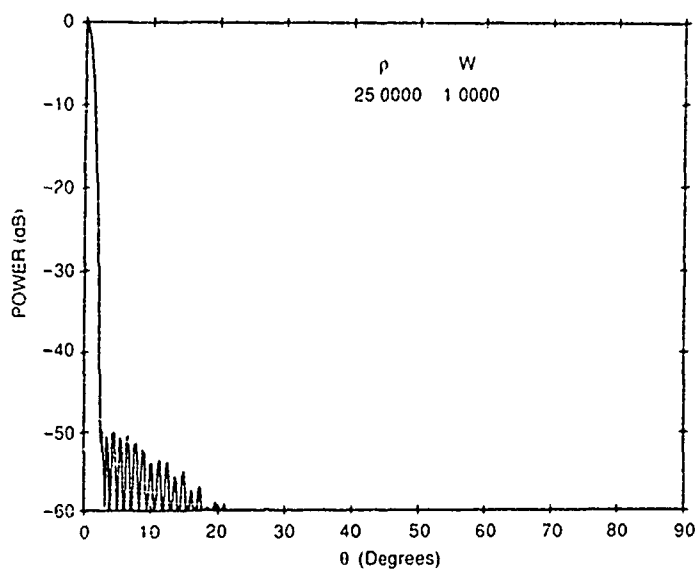
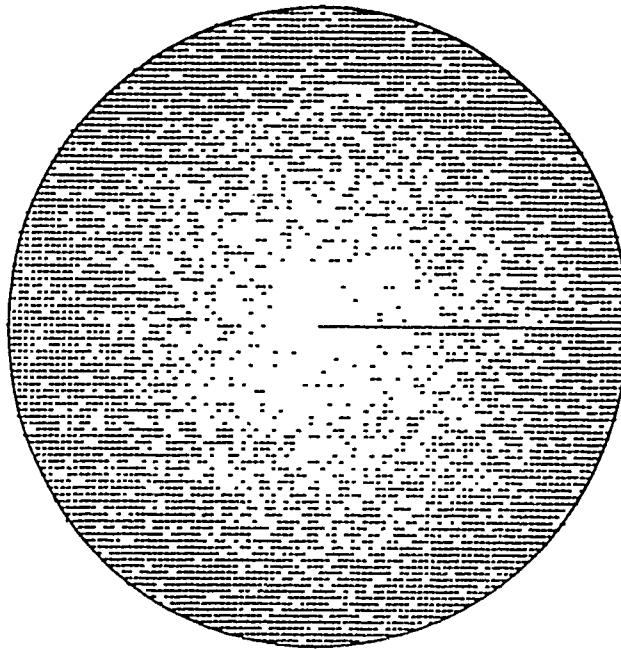(a) Power Pattern from –50 dB Taylor Taper Sampled for $d_x = d_y = \lambda/2$
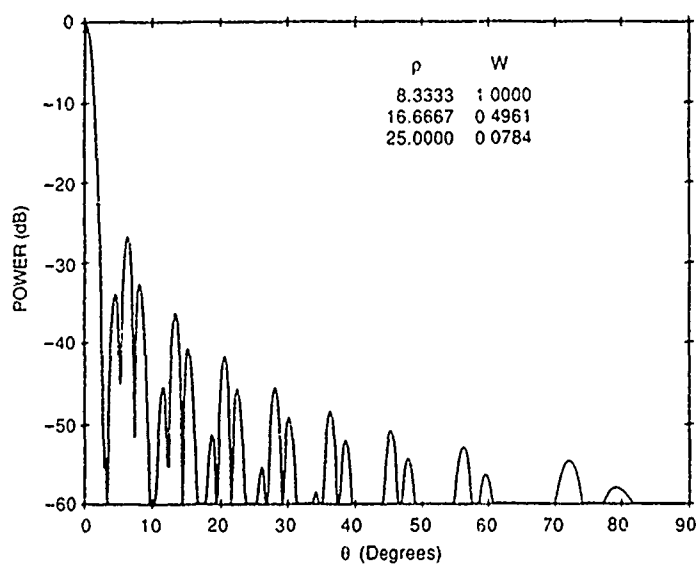
(b) Power Pattern from a Filled (Unthinned), 3-Step Distribution
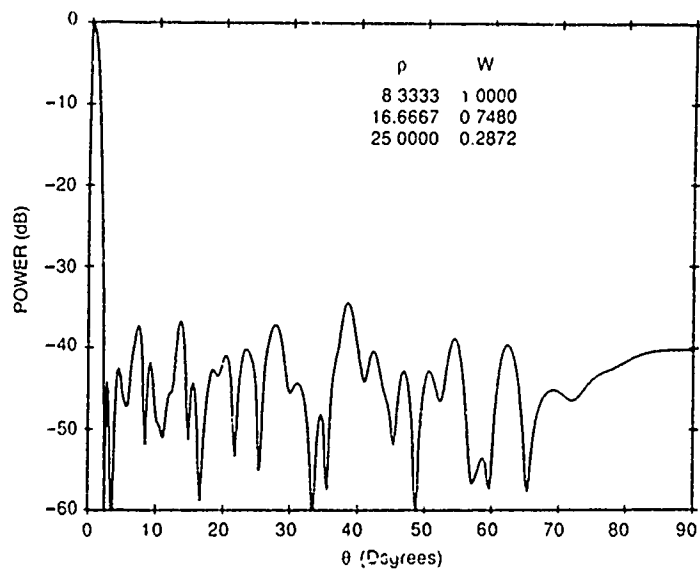
Figure 4.

17

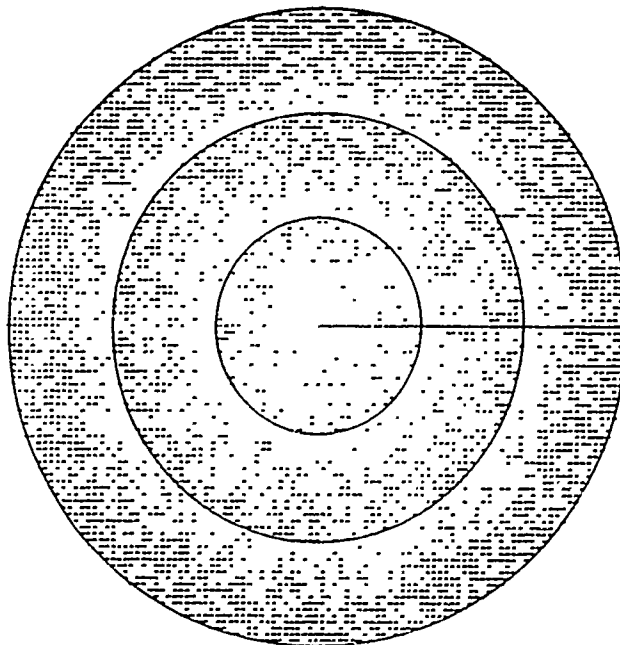(a) Power Pattern from a Thinned, 1-Step Distribution, Method 1

(b) Distribution of Non-Excited (Thinned) Elements for Figure 5a
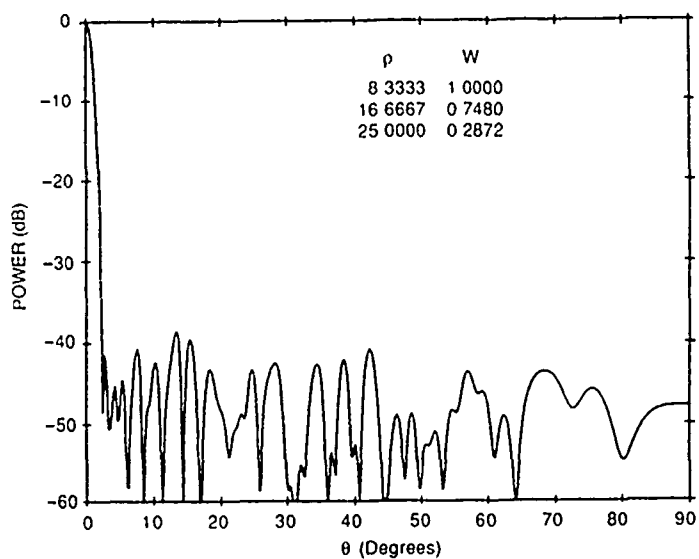
Figure 5.

ρ	W
8 3333	1 0000
16.6667	0 7480
25 0000	0.2872

(a) Power Pattern; 3-Step Distribution; Method 1

(b) Distribution of Non-Excited (Thinned) Elements for Figure 6a

Figure 6.

19

ρ	W
8 3333	1 0000
16 6667	0 7480
25 0000	0 2872

(a) Power Pattern; 3-Step Distribution; Method 2

(b) Distribution of Partially Excited Elements for Figure 7a

Figure 7.

(a) Power Pattern; 3-Step Distribution; Method 3
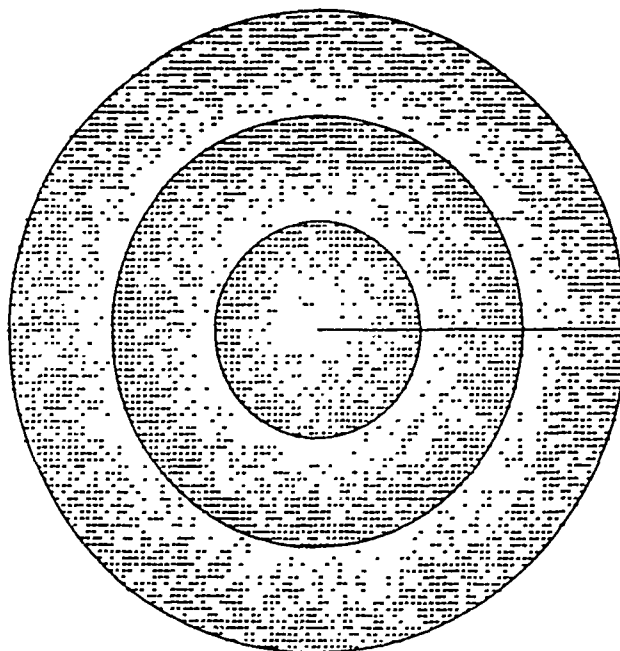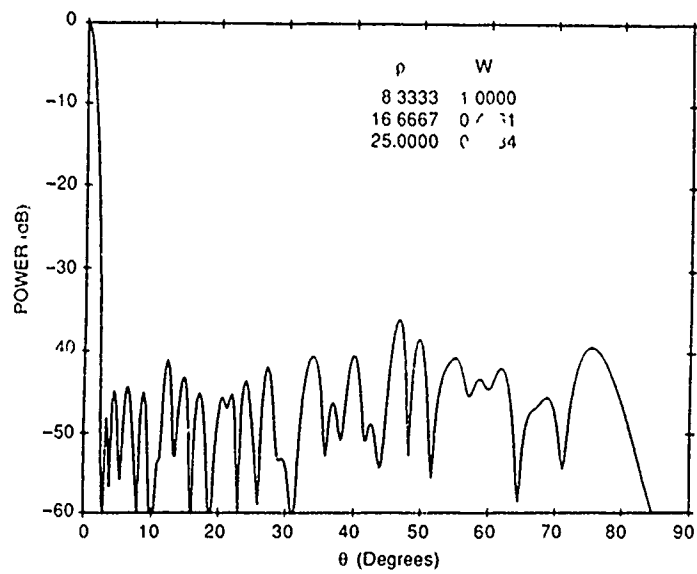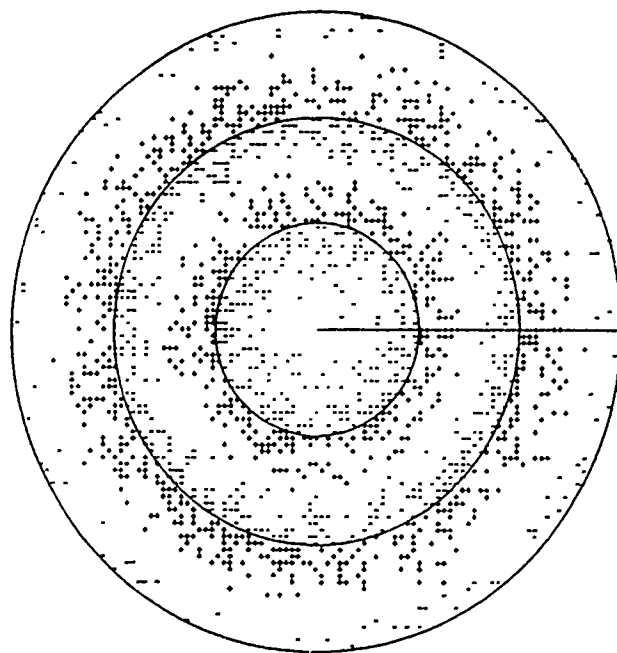

KIND= 3.0 NOTICE THAT N=50 IS ASSUMED HERE.

(b) Distribution of Elements with Increased (+) or Decreased (-) Excitation for Figure 8a

Figure 8.

21

element is excited at the level of the next (lower) step, and in 8b the plus signs indicate that the previous (higher) step level is used.

Figure 6a, 7a, and 8a show the results of applying the three algorithms to smooth the average amplitude illuminations. Apparently methods 2 and 3 have very similar results, with average sidelobe levels between -45 (Method 3) and -47 dB (Method 2). Method 1 has, as expected, the highest sidelobes, at -42.5 dB but these are substantially suppressed compared to the case of a single step (thinning with uniform amplitude) (Figure 5a). Peak sidelobes along the cut $\phi = 0$ range between -33 dB (Method 1) to -38 dB (Method 2).

Figures 6b, 7b, 8b show the state of the array aperture for the three methods. Figures 9 through 11 compare the results from the 3 synthesis approaches for a range of design sidelobe levels, and reveal some interesting differences among the methods. Figure 12 gives the directivity and selected $\bar{n}$ as a function of design sidelobe level. Figures 9, 10, and 11 each have three parts, and show normalized input power, directivity and average sidelobe level as a function of design sidelobe level for the three methods. Each figure shows data for one, two, four and six steps.

For one step, all of the data are the same; the three methods are identical, and equivalent to the Skolnik technique. As more steps are added, the three approaches become characteristically different. In almost all cases the input power and directivity decrease with decreased design sidelobes (as one would expect because of increased thinning) and the average sidelobe level increases for the same reason.

Figure 9 shows the directivity of an array synthesized by Method 1. Several additional data points have been added to this figure to compare the several directivity formulas Eq. (38) and Eq. (41) with the exact gain as computed by numerically performing the integral in Eq. (41). Two cases, representing design sidelobes of -30 dB and -60 dB were investigated for the array with a single step height, and a third case was evaluated for design sidelobes of -60 dB and six steps. The exact data are given by the circles, which are shown to be less than 0.2 dB from the plotted results using the formula (42). The results of using Eq. (39) are denoted by an asterisk. For one step and assuming element directivity of π, Eq. (39) leads to directivities between 0.9 and 1.0 dB higher than the exact number. For the case with one step, identical accuracies are obtained using Methods 1 and 2. For an array with six steps and Method 1 thinning, the results are closer, and here the results of using the formula (41) are within 0.3 dB of the correct value. Figure 10, computed using Method 2 thinning, shows only the integrated value (at -60 dB design sidelobe level and six steps). In this case all three methods yield results within 0.05 dB of each other. These results strongly support the use of Eq. (42), which is used throughout Figures 9, 10, and 11.

For Method 1 (Thinning), the average sidelobe reduction due to increasing the number of steps from one to six is about 8 dB, independent of the design sidelobe level. This is less true of Methods 2 and 3, both of which exhibit a wider spread of average sidelobe level as a function of the number of steps.

There is an interesting anomaly in the Method 3 data for two steps. As shown in Figure 11, the two-steps curve appears quite different from the curves for 1, 4, and 6 steps. The reason is that for Method 3 one must select both the step radius ρ_n and the step height V_n at each radius to define the stepped distribution. The method chosen for determining step height was to have the taper amplitude
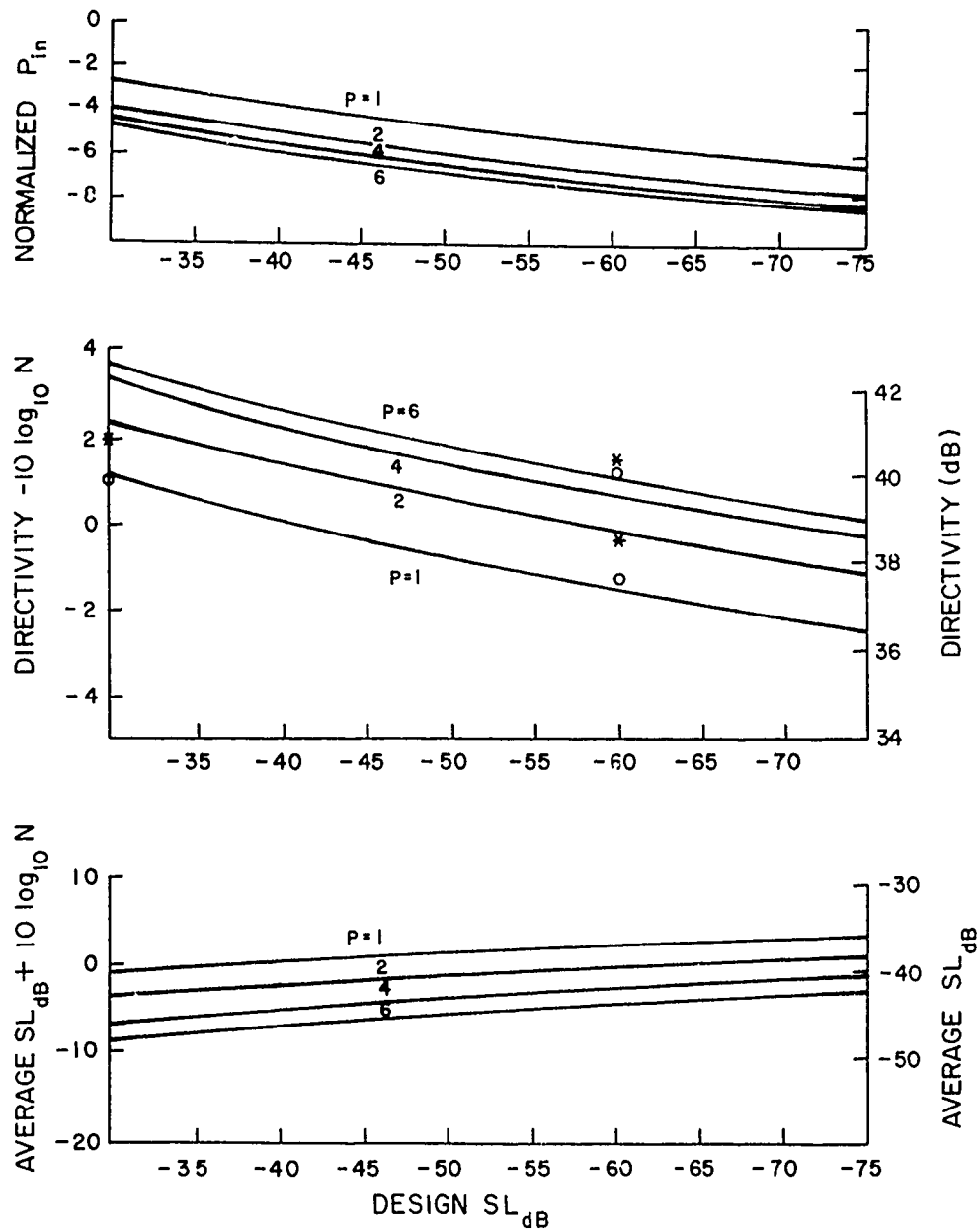
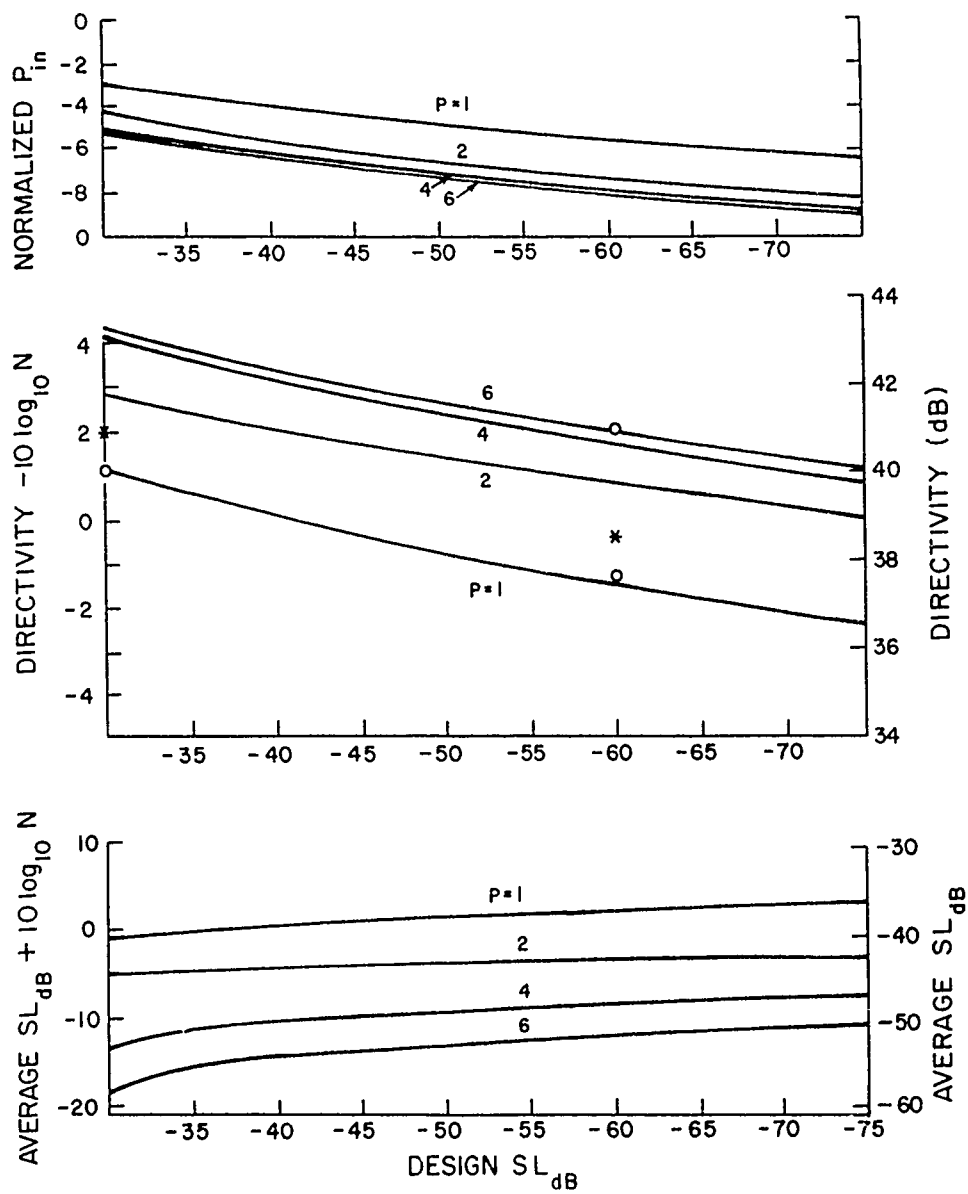Figure 9. P_{in}, Directivity, and Average SL vs Design SL; Method 1

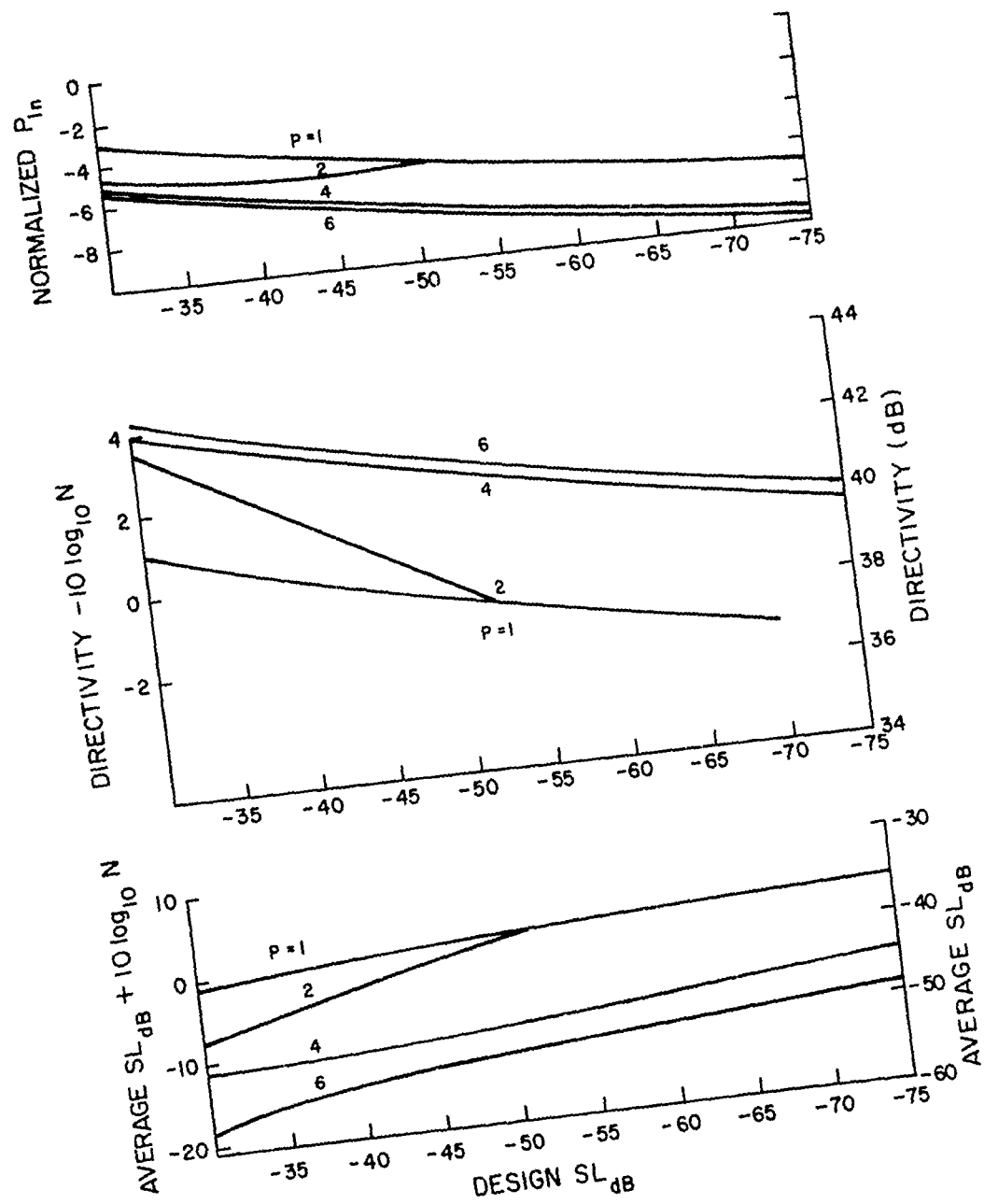Figure 10. P_{in}, Directivity, and Average SL vs Design SL; Method 2

Figure 11. P_{in}, Directivity, and Average SL vs Design SL; Method 3
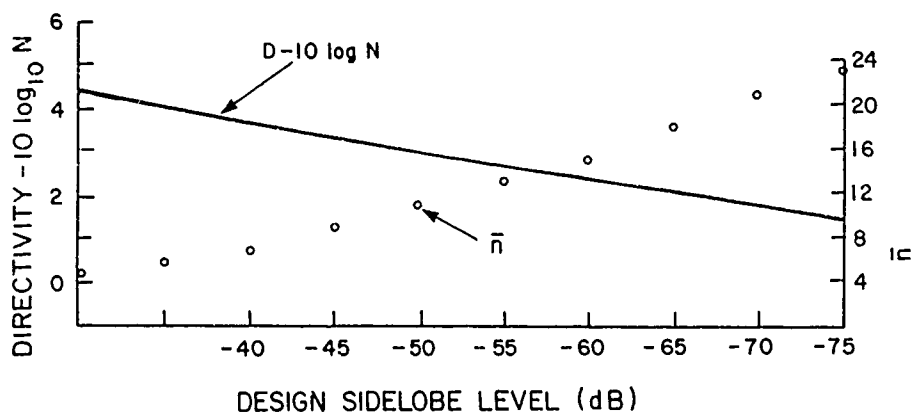
25

Figure 12. Taylor Directivity and Selected $\bar{n}$ vs Design SL

at the step radius equal the average value of two adjacent levels, namely,

$$A(\rho_p) = \frac{1}{2} [V_p + V_{p+1}] \, ,$$

$$V_p - A(\rho_p) = A(\rho_p) - V_{p+1} \, . \tag{49}$$

Selection of this condition was quite arbitrary, and works when there are enough steps. However, when there were only two steps and with low sidelobe aperture illuminations, this choice resulted in selection of a second step V_2 that would have gone below zero for design sidelobe levels less than -50 dB. To avoid this outcome, the height V_2 was set to a very small positive number. The net result, shown in Figure 11, is for the two step data of Method 3 to become essentially equal to the one-step data when the sidelobes become lower than -50 dB. This result occurs only for the two-step case, and indicates that one must exercise some care in choosing the step-heights for Method 3. Figure 12 shows the normalized directivity of the ideal Taylor pattern and is to be compared with Figures 9, 10 and 11. Note that several of the six-step configurations for Methods 2 and 3 have nearly the maximum available directivity. Figure 12 also shows the selected $\bar{n}$.

Figures 13a and 13b give additional perspective on array design. The figures show the variation of normalized EIRP with design sidelobe level for Methods 1 and 2 with one to six steps. Method 3 results, though not shown, are virtually the same as for Method 2. The remarkable fact illustrated is the near equality of EIRP for all methods at any given sidelobe level. The net spread of these curves is approximately 1 dB in all cases. So, in terms of EIRP, only the design sidelobe level is important, not the method used or the number of quantization levels (especially for greater than one level).
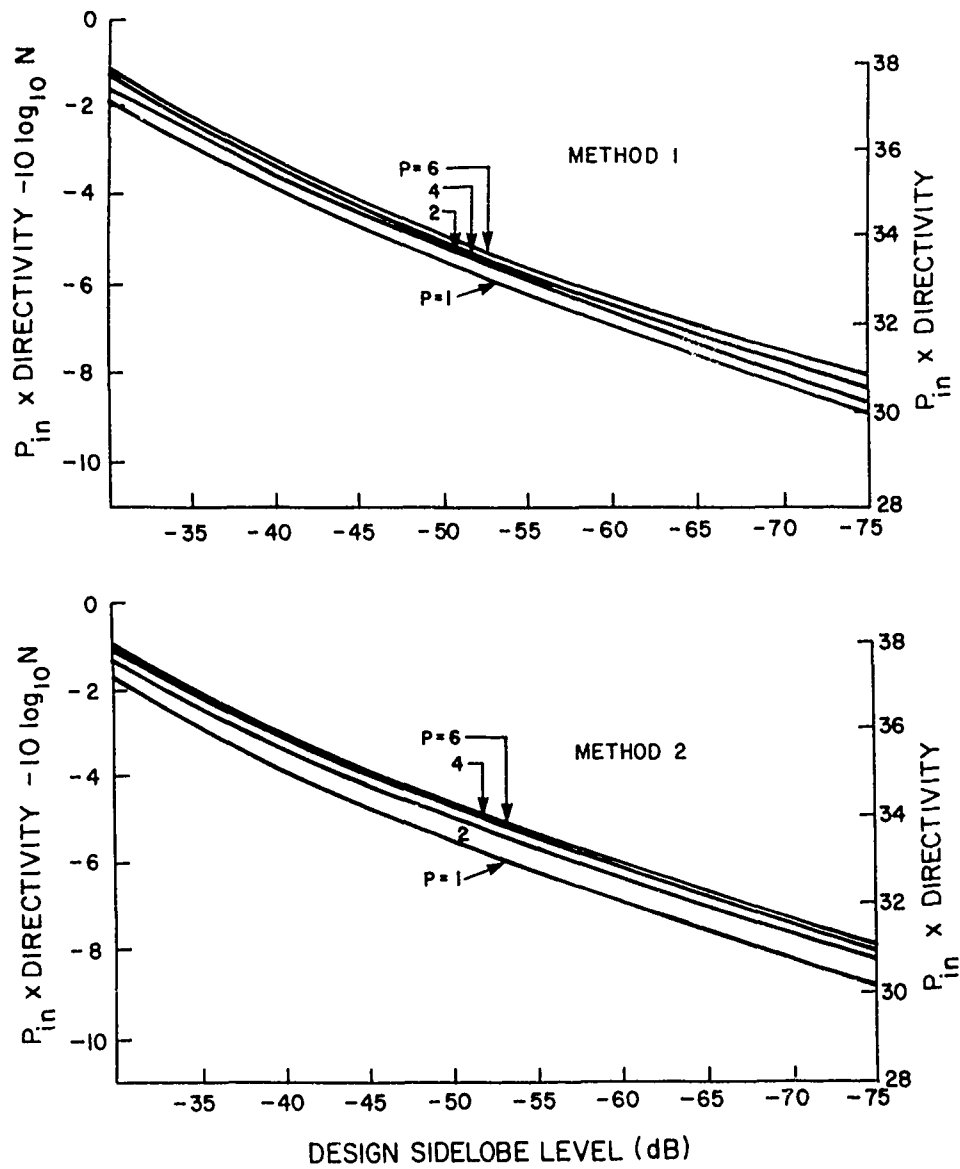
Figure 13. Normalized EIRP vs Design SL for Methods 1, 2 with 1-6 Steps

Figures 9c through 11c show average sidelobe levels as a function of the design sidelobe level for various numbers of steps. The plotted sidelobe level parameter is [Avg sl] dB $+$ 10 $\log_{10}$ N, and so the data is invariant with the number of filled array elements (once the array exceeds a minimum size) However, it is meaningless to select an illumination to produce (near) design sidelobes lower than the average sidelobe level, and so it is of interest to determine how large an array must be in order to sustain any given near and far sidelobe level. A good estimate of this quantity is obtained by setting the average sidelobe level equal to the design (peak) sidelobe level minus some margin. The offset, or margin, accounts for the fact that the peak sidelobes of the random distribution may be significantly above the statistical average level, and it is common practice to assume a margin of 10 to 20 dB depending on the percentage of sidelobes allowed to exceed the peak sidelobe estimate.

Using the normalized sidelobe data from Figures 9 and 10, Figures 14a and 14b are obtained by setting

$$SL_{dB} = SL_{norm} - 10 \log_{10} N$$

$$= SL_{design} - Margin_{dB} \tag{50}$$

for Margin dB a positive number. Solving for N yields:

$$10 \log_{10} N = SL_{norm} - SL_{design} + Margin_{dB} \tag{51}$$

To give the required array size, the figures are plotted for Methods 1 and 2 with design sidelobes (the peak Taylor sidelobes) set to values between –30 and –75 dB, and with Margin dB set to zero. Thus, Figure 14 gives the minimum array size required for the average sidelobe level to equal the design near-sidelobe level. Note that for P = 1 (one level) these cases reduce to the Skolnik et al result, and as shown in the reference, the average sidelobe level should be approximately equal to the number N of elements remaining in the highly thinned array. Figure 14 confirms the results for the arrays studied herein. The figure can be used for a non-zero margin by simply increasing N by the value of the desired margin, for example, by the factor 10 for each desired 10 dB of margin.

5. CONCLUSION

This report has investigated the use of statistical thinning and quantized element weights to produce low sidelobe patterns using large circular array apertures. The major results of the analysis show that by using either of several thinning algorithms it is possible to obtain substantial sidelobe reduction by a combination of statistical thinning and the use of discrete amplitude quantization.
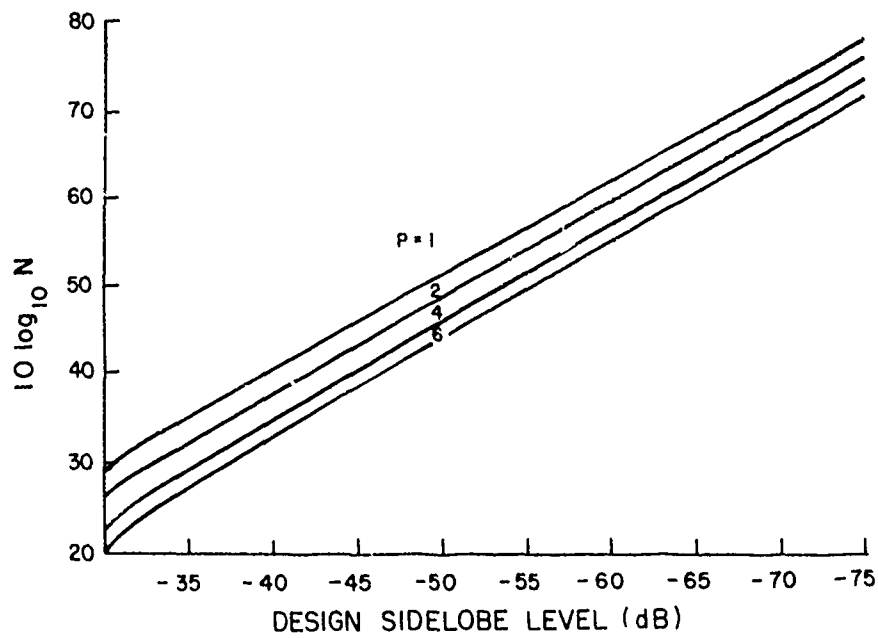
ARRAY ELEMENT COUNT N

(a) Number of Array Elements for Average SL = Peak SL; Method 1
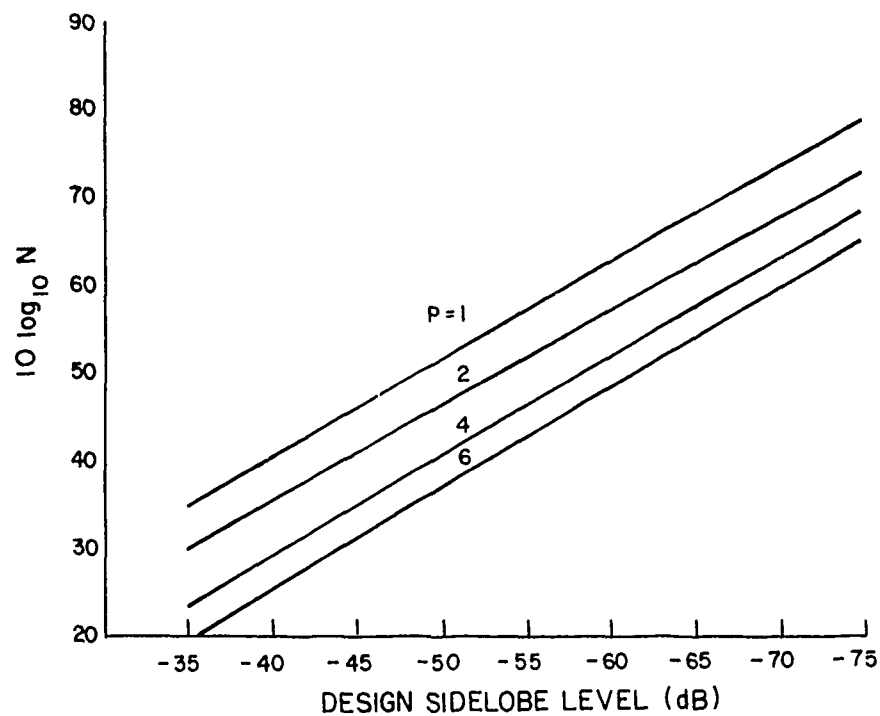
ARRAY ELEMENT COUNT N

(b) Number of Array Elements for Average SL = Peak SL; Method 2

Figure 14.

29

References

1. Skolnik, M., Sherman III, J.W., and Ogg, Jr., F.C. (1964) Statistically Designed Density - Tapered Arrays, *IEEE Trans. Antennas Propagat.* **AP-12**:408-411.

2. Lo, Y.T., (1964) A Mathematical Theory of Antenna Arrays with Randomly Spaced Elements, *IEEE Trans. Antennas Propagat.* **AP-12**:257-268.

3. Steinberg, B.D. (1972) The Peak Sidelobe of the Phased Array Having Randomly Located Elements, *IEEE Trans. Antennas Propagat.* **AP-20**(No. 2).

4. Numazaki, T., Mano, S., Kategi, T., and Mizusawa, M. (1987) An Improved Thinning Method for Density Tapering of Planar Array Antennas, *IEEE Trans. Antennas Propagat.* **AP-35** (No. 9):1066-1069.

5. Taylor, T.T. (1960) Design of Circular Apertures for Narrow Beamwidth and Low Sidelobes, *IRE Trans.* **AP-8**:23-26.

6. Hansen, R.C. (1983) *The Handbook of Antenna Design,* Vol 2, Chapter 10, pp. 157, Rudge et. al. (Editors), Peter Peregrinius Ltd.

Appendix

Variation of Average Sidelobe Level with Element Count (k = 1 Case)

It is of interest to scale the diameter of the aperture and, correspondingly, the radial dependence of the staircase function and the taper, while retaining the same $\lambda/2$ model mesh spacing. To effect this scaling, let

$$D \rightarrow cD,$$

$$r_p \rightarrow cr_p,$$

$$A(r) \rightarrow A(cr), \tag{A1}$$

$$d_x = d_y = 1/2 \qquad (\lambda/2 \text{ spacing}),$$

and

$$\{V_p : p = 1, 2, \ldots, P\} \text{ remains unchanged.}$$

As noted previously, the normalized average sidelobe level for Method 2 is given by

$$SL = \frac{P_{SL}}{P_{max}} = \frac{\displaystyle\sum_{p=1}^{P} \sum_{n(p)} \left\{ A_n (V_p + V_{p+1}) - V_p V_{p+1} \right\} - \sum_n A_n^2}{\left(\displaystyle\sum_n F_n \right)^2} \tag{A2}$$

The denominator is random, but even for "moderately large" arrays its ensemble average is nearly that from a single spatial realization resulting from Method 2 thinning. Thus,

$$\overline{\left(\sum_n F_n\right)^2} \approx \left(\sum_n F_n\right)^2 \Bigg|_{\substack{\text{any sample} \\ \text{array realization}}} . \tag{A3}$$

The first term in the numerator of SL is given by

$$S_1 = \sum_{p=1}^{P} \sum_{n(p)} \left\{ A_n (V_p + V_{p+1}) - V_p V_{p+1} \right\}. \tag{A4}$$

Taking account of the radial dependance of A_n, and interpreting S_1 dxdy as an area calculation using a two-dimensional rectangular quadrature, then transforming to polar coordinates yields

$$S_1 \approx (dx\, dy)^{-1} \int_0^{2\pi} d\phi \int_0^a dr\, r \left\{ A(r)\, v(r) - v(r) \right\}$$

$$= \left(\frac{2\pi}{dx\, dy}\right) a^2 \int_0^1 d\rho\, \rho \left\{ A(\rho)\, v(\rho) - v(\rho) \right\} \tag{A5}$$

$$= N'^2 \cdot 2\pi = \sum_{p=1}^{P} \left\{ \left(V_p + V_{p+1}\right) \int_{\rho_{p-1}}^{\rho_2} d\rho\, \rho\, A(\rho) - \frac{V_p V_{p+1}}{2} \left[\rho_p^2 - \rho_{p-1}^2\right] \right\}$$

$$\equiv N'^2 \lambda_p$$

where $N' = \frac{a}{d_x}$, $\rho_0 = 0$ and $\rho_1 = 1$. The integral of $\rho A(\rho)$ can be evaluated in closed form as follows. Substituting

$$A(\rho) = \sum_{m=0}^{\bar{n}-1} D_m J_0 (\pi \mu_m \rho) \tag{A6}$$

into the integral yields

$$\int_{\rho_{p-1}}^{\rho_p} d\rho\, \rho\, A(\rho) = \sum_{m=0}^{\bar{n}-1} \frac{D_m}{\pi \mu_m} \left\{ \rho_p J_1 (\pi \mu_m \rho_p) - \rho_{p-1} J_1 (\pi \mu_m \rho_{p-1}) \right\}.$$

This completes the determination of λ_p and the term S_1.

As shown above, the numerator of SL can be expressed as

$$\lambda_p N'^2 - \sum_n A_n^2 , \tag{A7}$$

where

$$\lambda_p = \lambda_p \left(\rho_{p,}, \bar{n}, P, \ldots \right)$$

but not N'. We are left with the evaluation of

$$\sum_n A_n^2 \qquad \text{and} \qquad \overline{\left(\sum_n F_n \right)^2} . \tag{A8}$$

For a circular Taylor taper,

$$A(r) = \sum_{m=0}^{\bar{n}-1} D_m J_0 \left(\pi \mu_m \frac{r}{a} \right) \tag{A9}$$

where $0 \leq r \leq a = N' d_x$. Letting, $P = r/a$ and approximating the area under $A^2_{(r)}$ with a rectangular quadrature, one obtains

$$\int_0^{2\pi} d\phi \int_0^a dr \, r \, A^2(r) \approx dx \, dy \sum_n A_n^2 \tag{A10}$$

which reduces to

$$\sum_n A_n^2 = \frac{2\pi}{dx \, dy} \, a^2 \sum_{m=0}^{\bar{n}-1} D_m^2 \int_0^1 d\rho \, \rho \, J_0^2 (\pi \mu_m \rho)$$

by virtue of orthogonality. The integral is readily evaluated in closed form. (See Van Bladel, p. 514, (23)), leading to

$$\sum_n A_n^2 = \pi N'^2 \sum_{m=0}^{\bar{n}-1} D_m^2 J_0^2 (\pi \mu_m)$$

$$= N'^2 C_2 . \tag{A11}$$

Thus far, one obtains

$$SL = \frac{\lambda_P N'^2 - C_2 N'^2}{\overline{\left(\sum_n F_n \right)^2}} . \tag{A12}$$

To evaluate the denominator, we note that

35

$$\overline{\left(\sum_n F_n\right)^2} = \overline{\sum_{n,n'} F_n \, F_n'}$$

$$= \sum_{n,n'} \overline{F_n \, F_n'}$$

$$= \sum_{\substack{n,n' \\ n \neq n'}} \overline{F_n \, F_n'} + \sum_n \overline{F_n^2}$$

$$= \sum_{\substack{n,n' \\ n \neq n'}} \overline{F}_n \, \overline{F}_n' + \sum_n \overline{F_n^2} \tag{A13}$$

$$= \sum_{\substack{n,n' \\ n \neq n'}} A_n A_n' + \sum_p \sum_{n(p)} \left\{ A_n \left(V_p + V_{p+1}\right) - V_p \, V_{p+1} \right\}$$

$$= \sum_{\substack{n,n' \\ n \neq n'}} A_n A_n' + \lambda_p N'^2$$

$$= \underbrace{\sum_{\substack{\text{all,} \\ n,n'}} A_n A_n' - \sum_n A_n^2 + \lambda_p N'^2}$$
$$= \text{numerator of SL}$$

It follows that

$$SL = \frac{1}{1 + \left[\dfrac{\displaystyle\sum_{\substack{\text{all,} \\ n,n'}} A_n A_n'}{\lambda_p N'^2 - C_2 N'^2} \right]} \ . \tag{A14}$$

Next, we must look closely at the sum

$$S_2 = \sum_{\substack{\text{all,} \\ n,n'}} A_n A_n'. \tag{A15}$$

and it will be useful to revert back to the original 2-dimensional array notation, namely,

$$A_n \rightarrow A_{n,m}$$

and

$$A_n' \rightarrow A_{n',m'}. \tag{A16}$$

The sum may now be written as

$$S_2 = \sum_{\substack{\text{all} \\ n, n' \\ m, m'}} A_{n,m} A_{n',m'}$$ (A17)

$$= \sum_n \sum_m \sum_i \sum_{i'} A_{n,m} A_{n+i, m+i'}$$

which is a 2-dimensional autocorrelation function.

Because of the circular symmetry of the Taylor function and the circular aperture, it is useful to convert the expansion to polar form. It is clear that the 2-dimensional displacement variables, i and i' must also be transformed to polar form. The "area" is, therefore, given by

$$d_x^2 \, d_y^2 \, S_2 \approx \int_0^{2\pi} d\theta \int_0^a d\tau\tau \int_0^{2\pi} d\phi \int_0^a dr \, r \, A(r) \, A(r+\tau)$$ (A18)

The change to dimensionless variables

$$\rho = r/a \quad \text{and} \quad \upsilon = \tau/a$$

yields

$$(dx \, dy)^2 \, S_2 \approx (2\pi)^2 \, (N' \, dx)^4 \int_0^1 d\upsilon \, \upsilon \int_0^1 d\rho \, \rho \, A(\rho) \, A(\rho+\upsilon)$$ (A19)

$$= (2\pi)^2 \, (N' \, dx)^4 \, I.$$

Since $dx = dy$ has been assumed, and $a = N' dx$, S_2 may be written as:

$$S_2 = 4\pi^2 I \, N'^4.$$ (A20)

Inserting into the expression for SL, we are led to

$$SL = \cfrac{1}{1 + \left(\cfrac{4\pi^2 I}{\lambda_p - C_2}\right) N'^2} \equiv \frac{1}{1 + C_s \, N'^2}$$ (A21)

$$= \cfrac{1}{1 + \left(\cfrac{4\pi I}{\lambda_p - C_2}\right) N}, \text{ since } N = \pi N'^2$$

Numerical studies show that to an excellent approximation

$$SL \sim O\left(\frac{1}{N}\right).$$ (A22)

where N is total number of nodes within (and on) the circular aperture.

The evaluation of the integral, I, can be accomplished efficiently and accurately by numerical means. Both the inner and outer integrals lend themselves well to low-order Gauss quadrature of

moments. Furthermore, $A(\rho)$ can be rapidly evaluated using the same cubic spline code that was discussed earlier for the "thinning" code. It should be apparent that C_s (l, λ_p, C_2) needs to be determined only when $\rho_l \neq l\Delta\rho$ is of interest. The results can be applied to arbitrary aperture diameters as long as $\rho_l = l\Delta\rho$.

MISSION
of
Rome Air Development Center

RADC plans and executes research, development, test and selected acquisition programs in support of Command, Control, Communications and Intelligence (C^3I) activities. Technical and engineering support within areas of competence is provided to ESD Program Offices (POs) and other ESD elements to perform effective acquisition of C^3I systems. The areas of technical competence include communications, command and control, battle management, information processing, surveillance sensors, intelligence data collection and handling, solid state sciences, electromagnetics, and propagation, and electronic, maintainability, and compatibility.